Journal of Power Sources 184 (2008) 104–119

Contents lists available at ScienceDirect

Journal of Power Sources

journal homepage: www.elsevier.com/locate/jpowsour

Review

A review of PEM fuel cell durability: Degradation mechanisms and mitigation strategies

Jinfeng Wu[a], Xiao Zi Yuan[a], Jonathan J. Martin[a], Haijiang Wang[a,*], Jiujun Zhang[a], Jun Shen[a], Shaohong Wu[a], Walter Merida[a,b]

[a] Institute for Fuel Cell Innovation, National Research Council of Canada, Vancouver, B.C., Canada V6T 1W5
[b] Department of Mechanical Engineering, University of British Columbia, Vancouver, B.C., Canada V6T 1Z4

ARTICLE INFO

Article history:
Received 20 March 2008
Received in revised form 3 June 2008
Accepted 4 June 2008
Available online 11 June 2008

Keywords:
PEM fuel cells
Durability
Degradation mechanism
Mitigation
Accelerated test

ABSTRACT

This paper reviews publications in the literature on performance degradation of and mitigation strategies for polymer electrolyte membrane (PEM) fuel cells. Durability is one of the characteristics most necessary for PEM fuel cells to be accepted as a viable product. In this paper, a literature-based analysis has been carried out in an attempt to achieve a unified definition of PEM fuel cell lifetime for cells operated either at a steady state or at various accelerated conditions. Additionally, the dependence of PEM fuel cell durability on different operating conditions is analyzed. Durability studies of the individual components of a PEM fuel cell are introduced, and various degradation mechanisms are examined. Following this analysis, the emphasis of this review shifts to applicable strategies for alleviating the degradation rate of each component. The lifetime of a PEM fuel cell as a function of operating conditions, component materials, and degradation mechanisms is then established. Lastly, this paper summarizes accelerated stress testing methods and protocols for various components, in an attempt to prevent the prolonged test periods and high costs associated with real lifetime tests.

Contents

* Corresponding author. Tel.: +1 604 221 3038; fax: +1 604 221 3001.
E-mail address: haijiang.wang@nrc-cnrc.gc.ca (H. Wang).

0378-7753/$ – see front matter © 2008 Elsevier B.V. All rights reserved.
doi:10.1016/j.jpowsour.2008.06.006

1. Introduction

To date, considerable effort has been devoted to the development of highly efficient and reliable polymer electrolyte membrane (PEM) fuel cells and stacks intended for many potential power source applications, including batteries for portable devices; fuel cell engines for automotive applications, displacing the internal combustion engine; and the residential stationary power market. Unquestionably, significant progress has been achieved over the past decade, especially in the areas of increasing volumetric and/or gravimetric specific power density and more effective materials utilization.

However, contrary to expectations held since the last decade that PEM fuel cells would be commercialized in stationary applications by 2001 and in transport applications as early as 2003 [1], technical challenges remain for the on-board storage and infrastructure for hydrogen fuel, as well as for the fuel cell system itself. With regard to the fuel cell system, one of the major hurdles is still its high cost; only when fuel cell costs are dramatically reduced to the US Department of Energy (DOE) target of $\$50\,kW^{-1}$ will fuel cells be competitive for virtually every type of power application.

Another technical barrier for the acceptance of fuel cells as a practical power source is durability under a wide range of operational conditions [2]. For different applications, the requirements for fuel cell lifetime vary significantly, ranging from 5000 h for cars to 20,000 h for buses and 40,000 h of continuous operation for stationary applications. Although the life targets for automobiles are much lower than those for stationary applications, the operating conditions of dynamic load cycling, startup/shutdown, and freeze/thaw make this goal very challenging for current fuel cell technologies. Unfortunately, at present most PEM fuel cell stacks provided by manufacturers and research institutes cannot achieve these goals.

The performance of a PEM fuel cell or stack is affected by many internal and external factors, such as fuel cell design and assembly, degradation of materials, operational conditions, and impurities or contaminants. Performance degradation is unavoidable, but the degradation rate can be minimized through a comprehensive understanding of degradation and failure mechanisms. In order to clearly understand the concepts of PEM fuel cell lifetime and performance decay discussed in this review, we first clarify several relevant terms [3–5]:

- *Reliability*: The ability of a fuel cell or stack to perform the required function under stated conditions for a period of time. It includes failure modes that can lead to catastrophic failure and performance below an acceptable level.
- *Durability*: The ability of a PEM fuel cell or stack to resist permanent change in performance over time. Durability decay does not lead to catastrophic failure but simply to a decrease in performance that is not recoverable or reversible (i.e., due to loss of electrochemical surface area, carbon corrosion, etc.). This issue is related to ageing.
- *Stability*: The ability to recover power lost during continuous operation. Stability decay is always concerned with operating conditions (such as water management) and reversible material changes.

The overall fuel cell performance decay rate, measured during continuous and uninterrupted operation, is the sum of both the stability and durability decay rates. Normal degradation targets require less than 10% loss in the efficiency of the fuel cell system at the end of life, and a degradation rate of 2–10 $\mu V\,h^{-1}$ is commonly accepted for most applications [6].

Table 1
Summary of steady state lifetime tests in the literature

Authors	Test time (h)	Degradation rate	Reference
Ralph	5,000	$4\,\mu V\,h^{-1}$	[7]
St-Pierre et al.	5,000	$1\,\mu V\,h^{-1}$	[8]
Washington	4,700	$6\,\mu V\,h^{-1}$	[9]
	8,000	$2.2\,\mu V\,h^{-1}$	
Endoh et al.	4,000	$2\,\mu V\,h^{-1}$	[10]
Yamazaki et al.	8,000	$2–3\,\mu V\,h^{-1}$	[11]
St-Pierre and Jia	11,000	$2\,\mu V\,h^{-1}$	[12]
Fowler et al.	1,350	$11\,\mu V\,h^{-1}$	[13]
Ahn et al.	1,800	$>4\,mV\,h^{-1}$	[14]
Cheng et al.	4,000	$3.1\,\mu V\,h^{-1}$	[15]
Scholta et al.	2,500	$20\,\mu V\,h^{-1}$	[16]
Cleghorn et al.	26,300	$4–6\,\mu V\,h^{-1}$	[4]

In this paper, studies conducted by academic and industry researchers on the lifetime of state-of-the-art PEM fuel cells operated in steady state or accelerated conditions such as load or thermal cycles or fuel or oxidant starvation are summarized. The major findings from both experimental and theoretical studies of the degradation and failure modes of fuel cells and their components are introduced. Feasible strategies to mitigate the performance decay resulting from each degradation mechanism are discussed in detail. The existing methods for accelerated stress testing of different components are analyzed. From the viewpoint of practical applications, a statistical model based on the accelerated lifetime data of fuel cell components is proposed to estimate real lifetime under normal testing conditions.

2. Steady state and accelerated lifetime tests

Until now, while comprehensive experimental results and reviews have been published in an attempt to understand the degradation mechanisms of fuel cell components such as electrocatalysts, membranes, and bipolar plates, only a relatively small number of studies aimed at real PEM fuel cell lifetimes have been conducted, due to the high costs and prolonged testing periods required. For example, more than 4.5 years of uninterrupted testing is needed to reach the 40,000-h lifetime requirement for a fuel cell system for stationary applications. For testing a fuel cell bus system (275 kW) for 20,000 h, the fuel expense alone would be approximately US $2 million (3.8 billion liters of hydrogen at US $\$5.3\,m^{-3}$). To increase sample throughput and reduce the experimental time required, several fuel cell developers and companies, such as Ballard Power Systems, DuPont, Gore, and General Motors, have proposed and implemented different accelerated stress tests (ASTs) to determine the durability and performance of current fuel cell components. This study summarizes papers published in the last decade on PEM fuel cell degradation and lifetimes. Tables 1 and 2 present work on steady state and accelerated lifetime tests, respectively.

Although most experiments on fuel cell lifetime under steady state operation demonstrated acceptable results, with a degradation rate between 2 and 10 $\mu V\,h^{-1}$, they were conducted for much less than 40,000 h. As for ASTs, almost all degradation rates were greater than 10 $\mu V\,h^{-1}$. Prior to commercializing fuel cell technology, more thorough studies on components and the analysis of system failure modes are imperative.

Table 2
Summary of accelerated durability tests in the literature

Authors	Test time (h)	Degradation rate	Operating conditions	Reference
Sishtla et al.	5,100	6 μV h^{-1}	Reformate fuel	[17]
Nakayama	4,000	4.3 μV h^{-1}	Reformate fuel	[18]
Isono et al.	2,000	10 μV h^{-1}	Reformate fuel	[19]
Maeda et al.	5,000	6 μV h^{-1}	Reformate fuel	[20]
Sakamoto et al.		50–90 μV	Per start/stop cycles	[21]
Fowler et al.	600	120 μV h^{-1}	Humidity cycles	[22]
Cho et al.		4200 μV	Per thermal cycles	[23]
Knights et al.	13,000	0.5 μV h^{-1}	Methane reformate fuel Low humidification	[6]
Oszcipok et al.		22,500 μV	Per cold start-up	[24]
Xie et al.	1,916	60 μV h^{-1}	Over-saturated humidification	[25]
	1,000	54 μV h^{-1}		
Yu et al.	2,700	21 μV h^{-1}	Low humidification	[26]
Endoh et al.	3,500	3 μV h^{-1}	High temperature Low humidification	[27]
Du et al.	1,900	70–800 μV h^{-1}	Cold start and hot stop	[28]
Xu et al.	1,000	<10 μV h^{-1}	High temperature Low humidification	[29]
Owejan et al.		0.212 mV	Per start/stop cycles	[30]

3. Major failure modes of different components of PEM fuel cells

3.1. Membrane

In a typical PEM fuel cell, the membrane is sandwiched between two catalyzed electrodes to transport the protons, support the anode and cathode catalyst layers, and more importantly, separate the oxidizing (air) and reducing (hydrogen) environments on the cathode and anode sides, respectively. Therefore, the requirements for an excellent membrane are manifold and stringent, including high protonic conductivity, flow reactant gas permeability, thermal and chemical stability, and so on [31]. The most commonly used and promising membranes for PEM fuel cells are perfluorosulfonic acid (PFSA) membranes such as Nafion® (Dupont™), Gore-Select® (Gore™), and Aciplex® and Flemion® (Asahi™). Extensive studies have been carried out on the mechanisms of membrane degradation and failure in the fuel cell environment. At present, however, unsatisfactory durability and reliability of the membrane is still one of the critical issues impeding the commercialization of PEM fuel cells.

3.1.1. Membrane degradation mechanisms

3.1.1.1. Mechanical degradation of the membrane. Membrane degradation can be classified into three categories: mechanical, thermal, and chemical/electrochemical [32,33]. Among them, mechanical degradation causes early life failure due to perforations, cracks, tears, or pinholes, which may result from congenital membrane defects or from improper membrane electrode assembly (MEA) fabrication processes. The local areas corresponding to the interface between the lands and channels of the flow field or the sealing edges in a PEM fuel cell, which are subjected to excessive or non-uniform mechanical stresses, are also vulnerable to small perforations or tears. During fuel cell operation, the overall dimensional change due to non-humidification [34], low humidification [6,26,35,36], and relative humidity (RH) cycling [37] are also detrimental to mechanical durability. The constrained membrane in an assembled fuel cell experiences in-plane tension resulting from shrinkage under low RH and in-plane compression during swelling under wet conditions. The migration and accumulation of the catalysts and the decomposition of the seal into the membrane, as described in Sections 3.2.1 and 3.5, also negatively affect membrane conductivity and mechanical strength, significantly reducing ductility. A physical breach of the membrane due to local pinholes and perforations can result in crossover of reactant gases into their respective reverse electrodes. If this happens, the highly exothermic direct combustion of the oxidant and reductant occurs on the catalyst surface and consequently generates local hot-points. A destructive cycle of increasing gas crossover and pinhole production is then established, which undoubtedly accelerates degradation of the membrane and the entire cell. The results of Huang et al. [37] suggested that mechanical failure of the membrane starts as a random, local imperfection that propagates to catastrophic failure.

3.1.1.2. Thermal degradation of the membrane. In order to maintain well-hydrated PFSA membranes, the most favorable working temperature of a PEM fuel cell is usually from 60 to 80 °C. Conventional PFSA membranes are subject to critical breakdown at high temperatures due to the glass transition temperatures of PFSA polymers at around 80 °C. However, rapid startup, stable performance, and easy operation in subfreezing temperatures are necessary capabilities for fuel cell technologies to achieve prior to commercialization in vehicles and portable power supply applications. On the other hand, much effort has been made recently to develop PEM fuel cells that operate above 100 °C, in order to enhance electrochemical kinetics, simplify water management and cooling systems, and improve system CO tolerance. Membrane protonic conductivity drops significantly with the decrease in water content when the fuel cell is operated at high temperatures [38] and under low humidity [39].

Several studies have addressed the issue of thermal stability and thermal degradation of PFSA membranes. The polytetrafluoroethylene (PTFE)-like molecular backbone gives Nafion membranes their relative stability until beyond 150 °C due to the strength of the C–F bond and the shielding effect of the electronegative fluorine atoms [40]. At higher temperatures, Nafion begins to decompose via its side sulfonate acid groups. The thermal stability of Nafion was investigated by Surowiec and Bogoczek [41] using thermal gravimetric analysis, differential thermal analysis, and Fourier transform infrared spectroscopy, and only water was detected below 280 °C. At temperatures above 280 °C, sulfonic acid groups were spilt off. In their studies on the effect of heating Nafion onto platinum (Pt) in air, Chu et al. [42] found that sulfonic acid groups were lost after heating at 300 °C for 15 min, while Deng et al. [43], measured small amounts of sulphur dioxide up to 400 °C. Detailed mechanisms for PFSA thermal degradation were proposed by Wilkie et al. [40] and Samms et al. [44], including initiative rupture of the C–S bond to produce

sulphur dioxide, OH• radicals, and a left carbon-based radical for further cleavage at higher temperatures.

In order for fuel cells to be successfully commercialized for automotive and portable applications, membranes must be able to tolerate freezing temperature as well as thermal cycling. Several studies on the state of water in PFSA membranes below freezing have been conducted. Kim et al. [45] suggested that three different states of water exist in the membrane and that the "free water", which was not intimately bound to the polymer chain, would freeze below 0 °C. In addition, Cappadonia et al. [46] and Sivashinsky and Tanny [47] found that only a part of the water present in Nafion underwent freezing. Cho et al. [23] reported that the contact resistance between the membrane and the electrode increased after thermal cycles, whereas membrane ionic conductivity itself was not affected. However, McDonald et al.'s [48] results illuminated that, after 385 temperature cycles between +80 and −40 °C, ionic conductivity, gas impermeability, and the mechanical strength of Nafion membranes were severely impaired, although no catastrophic failures were detected. The phase transformation and volume change of water due to freeze/thaw cycles has a detrimental effect on the membrane's lifetime. To avoid this, proposed mitigation strategies include gas purging and solution purging to remove residual water during fuel cell startup and shutdown, which will be described in Section 3.1.2.

3.1.1.3. Chemical/electrochemical degradation of the membrane. The rates of hydrogen and air crossover to opposite sides of the membrane have been proved to be relatively slow and to result in only a 1–3% loss in fuel cell efficiency [49,50]. However, the aforementioned highly exothermal combustion between H_2 and O_2 can possibly lead to pinholes in the membrane, destroying the MEA and causing catastrophic problems. More severely, the chemical reaction on the anode and cathode catalysts can produce peroxide (HO•) and hydroperoxide (HOO•) radicals, which are commonly believed to be responsible for chemical attack on the membrane and catalysts [51,52]. Further investigation has also revealed that the generation of these radicals as well as the chemical degradation of the membrane is accelerated when the fuel cell is operated under open circuit voltage (OCV) and low humidity conditions [36]. Several mechanisms have been proposed, with conflicting views on whether the radicals are formed at the anode, at the cathode, or on both sides of the membrane. Some studies have shown that the loss of ionic groups begins at the anode side of the membrane and progresses towards the cathode [53,54], but Pozio et al. [55] and other researchers [56,57] have provided evidence of predominant cathode degradation. However, Mattsson et al.'s [58] observed no noticeable difference between the anode and cathode sides.

The presence of foreign cationic ions can significantly decrease cell performance by adsorbing on the membrane or catalysts. Possible sources of ultivalent ion contaminants include corrosion of stack components and impurities in the air stream, humidifier reservoirs, etc. [59]. Many cations showed stronger affinity than H^+ with the sulfonic acid group in PFSA membranes [60]. When the fuel cell was operating, more active sites were occupied by the ultivalent ions and, as a consequence, the membrane bulk properties, such as membrane ionic conductivity, water content, and H^+ transference numbers, changed proportionally to the cation ionic charge [61]. This effect is not normally serious unless the contamination concentration goes beyond 50% of sulfonic acid groups in the membrane [60]. The second possible mode of membrane deterioration due to contaminant ions comes from the altered water flux inside the membrane, and in this case, only 5% contaminant is sufficient. The displacement of H^+ with foreign cations also results in attenuated water flux and proton conductivity, and leads to much faster or more extensive membrane dehydration, especially near the anode [2]. Contamination by trace metal ions originating from the corrosion of metal bipolar plates or end plates, such as Fe^{2+} and Cu^{2+}, can strongly accelerate membrane thinning and performance decay of a PEM fuel cell by catalyzing the radicals' formation reactions, as shown in following equations [49]:

$$H_2O_2 + Fe^{2+} \rightarrow HO^{\bullet} + OH^- + Fe^{3+} \quad (1)$$

$$Fe^{2+} + HO^{\bullet} \rightarrow Fe^{3+} + OH^- \quad (2)$$

$$H_2O_2 + HO^{\bullet} \rightarrow HO_2^{\bullet} + H_2O \quad (3)$$

$$Fe^{2+} + HO_2^{\bullet} \rightarrow Fe^{3+} + HO_2^- \quad (4)$$

$$Fe^{3+} + HO_2^{\bullet} \rightarrow Fe^{2+} + H^+ + O_2 \quad (5)$$

As described above, this mechanism can lead to membrane thinning or the formation of pinholes and eventually to the catastrophic failure of the fuel cell.

Depending on the type of membrane, the HO• and HOO• radicals generated during the reaction can attack the α-carbon of an aromatic group, the ether links, or the branching points of the polymer. As for the PFSA membranes, the small quantity of carboxylate end groups with H-containing terminal bonds, which are inevitably formed during the polymer manufacturing process, are regarded as the inducing agent for membrane chemical decay due to its susceptibility to radical attack. One generally accepted mechanism, the unzipping reaction, initiates the abstraction of hydrogen from the end groups, releases HF, CO_2 and forms new carboxylate groups at the chain ends [61]. An example of radical attack on an end group of $-CF_2COOH$ is shown below [62].

$$R_f\text{–}CF_2COOH + {}^{\bullet}OH \rightarrow R_f\text{–}CF_2^{\bullet} + CO_2 + H_2O \quad (6)$$

$$R_f\text{–}CF_2^{\bullet} + {}^{\bullet}OH \rightarrow R_f\text{–}CF_2OH \rightarrow R_f\text{–}COF + HF \quad (7)$$

$$R_f\text{–}COF + H_2O \rightarrow R_f\text{–}COOH + HF \quad (8)$$

As the process repeats, the attack may propagate along the main chain, and eventually the polymer decomposes into low-molecular weight compounds. Another possible mechanism proposed by Endoh et al. [27] is the scission of the polymer main chains, in which the ether linkages are suggested to be the most susceptible side chain sites to radical attack, producing vulnerable –COOH groups. As a result, the average molecular weight of the polymer decreases while the number of –COOH groups increase with time. Even without susceptible end groups, under exposure to H_2, the polymer backbone of the PFSA membrane may preferentially react as follows [2]:

$$-CF_2- + 2H_2 \rightarrow -CH_2- + 2HF \quad (9)$$

Following this reaction, the radicals attack the resulting $-CH_2-$ groups. The rate of fluoride loss has been considered an excellent measurement of PFSA membrane degradation [63].

3.1.2. Mitigation strategies for membrane degradation

To prevent mechanical failure of the membrane, the MEA and flow field structure must be carefully designed to avoid local drying of the membrane [64,65], especially at the reactant inlet area [66]. A membrane reinforced with e-PTFE, developed by Gore Fuel Cell Technologies, exhibited a lifetime an order of magnitude longer than a non-reinforced membrane of comparable thickness [63], as shown in Fig. 1. Similar results for enhanced membrane mechanical strength were reported by Wakizoe et al. [67] and Xu et al. [29] using reinforced Aciplex® membranes and Nafion®–Teflon®–phosphotungstic acid composite membranes, respectively.

Several review papers [68–71] have covered the recent PEM development and fabrication approaches focusing on achieving

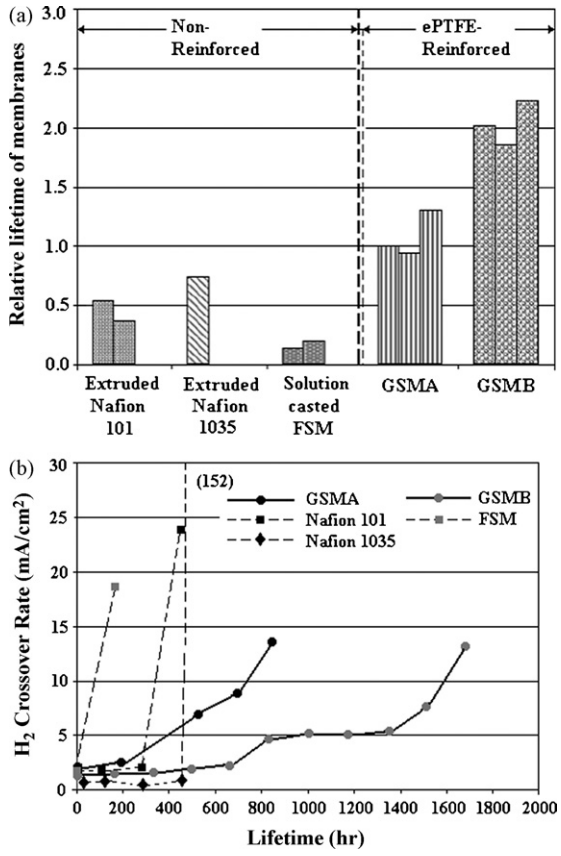

Fig. 1. Comparison of Gore reinforced membranes and non-reinforced membranes. (a) Lifetime of various membranes in accelerated fuel cell conditions; (b) H_2 crossover rate as a function of time. (Modified from [63] with permission.)

prolonged durability above 100 °C. The membranes developed so far can be classified into three groups: (1) modified PFSA membranes, which are swelled with nonvolatile solvents or incorporate hydrophilic oxides and solid inorganic proton conductors; (2) alternative sulfonated polymers and their composite membranes, such as SPSF, SPEEK, PBI, and PVDF; and (3) acid–base polymer membranes, such as phosphoric acid-doped Nafion®–PBI composite membranes.

With respect to the chemical and electrochemical degradation of the membrane, developing membranes that are chemically stable against peroxy radicals has drawn particular attention. Firstly, one solution is to develop novel membranes with higher chemical stability, such as a radiation-grafted FEP-g-polystyrene membrane [72,73], in which polystyrene was used as a sacrificial material owing to its low resistance to radicals [57]. Free-radical stabilizers and inhibitors such as hindered amines or antioxidants also have the potential to be mingled during membrane fabrication. Secondly, increased chemical stability can also be realized by modifying the structure of the available membrane. Curtin et al. [62] suggested that radical attack of the residual H-containing terminal bonds of the main chain of the PFSA membrane was the primary degradation mechanism. By eliminating the unstable end group, chemical stability was significantly enhanced [62]. Thirdly, the damage caused by hydrogen peroxide can be suppressed by redesigning the MEA. For example, a composite membrane suggested by Yu et al. [57], in which a thin recast Nafion membrane was bonded with a polystyrene sulfonic acid (PSSA) membrane, when positioned at the cathode of the cell could successfully prevent oxidation degradation of the PSSA membrane. Fourthly, introduction of peroxide-decomposition catalysts like heteropoly acids within the membrane has proven to moderate or eliminate membrane deterioration due to peroxide [74,75]. However, the advantage of this approach would be partially counteracted by a decrease in membrane stability and conductivity caused by the mixture of the catalysts. Last but not least, the development and implementation of new metal coatings with improved corrosion resistance and of catalysts that produce less hydrogen peroxide are long-term goals for membrane durability enhancement.

3.2. Electrocatalyst and catalyst layer

Pt and binary, ternary, or even quaternary Pt-transition metal alloys, such as PtCo, Pt–Cr–Ni, and Pt–Ru–Ir–Sn, supported on conductive supports have been proposed and implemented as electrocatalysts in PEM fuel cells. Commonly used supports include high-surface-area carbon materials, such as Vulcan-XC 72, Ketjen black, or Black pearls BP2000. These catalysts are in principle able to meet the performance and cost requirements for high-volume fuel cell applications. However, from a catalyst durability viewpoint, the performance of currently known materials is still unsatisfactory under harsh operating conditions, including high humidity, low pH values, elevated temperature, and dynamic loads in combination with an oxidizing or reducing environment [59].

3.2.1. Electrocatalyst and catalyst layer degradation mechanisms

Considerable effort has been put into the detailed examination of the mechanism of Pt catalyst degradation under long-term operation. Firstly, a pure Pt catalyst may be contaminated by impurities originating from supply reactants or the fuel cell system [50]. Also, the catalyst may lose its activity due to sintering or migration of Pt particles on the carbon support, detachment and dissolution of Pt into the electrolyte, and corrosion of the carbon support. Several mechanisms have been proposed to explain the coarsening in catalyst particle size during PEM fuel cell operation: (1) small Pt particles may dissolve in the ionomer phase and redeposit on the surface of large particles, leading to particle growth, a phenomenon known as Ostwald ripening [76]. On the other hand, the dissolved Pt species may diffuse into the ionomer phase and subsequently precipitate in the membrane via reduction of Pt ions by the crossover hydrogen from the anode side, which dramatically decreases membrane stability and conductivity [77]; (2) the agglomeration of platinum particles on the carbon support may occur at the nanometer scale due to random cluster–cluster collisions, resulting in a typical log-normal distribution of particles sizes with a maximum at smaller particle sizes and a tail towards the larger particle sizes [78]; (3) the growth in catalyst particles may also take place at the atomic scale by the minimization of the clusters' Gibbs free energy. In this case, the particle size distribution can be characterized by a tail towards the smaller particle sizes and a maximum at larger particle sizes [79]. However, so far, there is still no agreement on which mechanism is dominantly responsible for the catalyst particle growth [80]. Coarsening of the catalyst due to movement of its particles and coalescence on the carbon support can cause the catalytically active surface area to decrease [81]. Lastly, the formation of metal oxides at the anode [15] or cathode [14] side probably leads to an increase in particle sizes and ultimately results in a decrease in catalyst activity.

Corrosion of the catalyst carbon support is another important issue pertaining to electrocatalyst and catalyst layer durability that has attracted considerable attention lately in academic as well as in industry research [6,82,83]. In PEM fuel cells and stacks, two modes are believed to induce carbon corrosion: (1) transitioning between startup and shutdown cycles and (2) fuel starvation due to the blockage of H_2 from a portion of the anode under steady state conditions. The first mode, referred to as air-fuel front, can

be caused by non-uniform distribution of fuel on the anode and crossover of oxygen through the membrane, which is likely to occur during startup and shutdown of the PEM fuel cell. For the second mode, fuel starvation in individual cells may result from uneven flow sharing between cells during high overall stack utilization or from gas flow blockage attributed to ice formation when fuel cells work in subfreezing temperatures. In both cases, the anode electrode is partially covered with hydrogen and, under the circumstances of hydrogen exhaustion, the anode potential will be driven negative until water and carbon oxidation takes place according to the following equations [2]:

$$2H_2O \leftrightarrow O_2 + 4H^+ + 4e^- \quad E^\circ = 1.229V_{RHE} \tag{10}$$

$$C + 2H_2O \rightarrow CO_2 + 4H^+ + 4e^- \quad E^\circ = 0.207V_{RHE} \tag{11}$$

Despite the thermodynamic instability, carbon corrosion in a normal PEM fuel cell is negligible at potentials lower than 1.1 V vs. reversible hydrogen electrode (RHE) due to its slow kinetics. However, recent experiments have confirmed that the presence of electrocatalysts like Pt/C or PtRu/C can accelerate carbon corrosion and reduce the potentials for carbon oxidation to 0.55 V (vs. RHE) or lower [84]. When provided with sufficient water in the fuel cell, carbon is actually protected from corrosion by virtue of the H_2O oxidation process, unless the water in the electrode is depleted or the cell is subjected to a high current density not sustainable by water oxidation alone [28]. According to Eq. (8), cell reversal as a result of fuel starvation has a potential impact on the durability of the catalyst layer, the gas diffusion layer, or even the bipolar plate. As a consequence, the relative percentage of conductive material in the electrode may drop and the contact resistance with the current collector, as well as the internal resistance of the cell, will eventually increase. More seriously, the number of sites available to anchor the catalyst decreases with carbon corrosion, causing catalyst metal sintering [85], and in the extreme, a structural collapse of the electrode.

Another noteworthy hazard to PEM fuel cell durability at subzero temperatures is the influence of the phase transformation and volume changes of water on the physical properties of the membrane/electrode interface and electrode structure, in addition to the membrane. Cho et al. [23] observed a performance degradation rate of about 2.3% per freeze–thaw cycle from 80 to −10 °C. The cell performance degradation seen with thermal cycles was attributed to the physical damage of the electrode structure and MEA integrity resulting from ice expansion during freezing. The analytical results of McDonald et al. [48] demonstrated the relationship of temperature cycling between 80 and −40 °C to membrane structure, water management, ionic conductivity, gas permeability, and mechanical strength. A detailed summary of research on PEM fuel cell freeze and rapid startup can be found in Ref. [86].

Experimental results from Xie et al. [25] have also revealed the change in hydrophobic characteristics of the catalyst layer over time due to the dissolution of Nafion or PTFE, which detrimentally affects the water management and mass transport ability of the electrode.

3.2.2. *Mitigation strategies for electrocatalyst and catalyst layer degradation*

Recent research has proposed and successfully employed several strategies to enhance catalyst durability. First of all, fuel cell operating conditions play a major role in catalyst degradation. The dissolution of Pt from the carbon support is less favorable at low electrode potentials, which makes Pt catalysts more stable at the anode electrode than that at the cathode side. The experimental results of Mathias et al. [85] showed that the loss in Pt active surface area associated with an increase in testing time can be significantly decreased by operating the cell at low RH and low temperature,

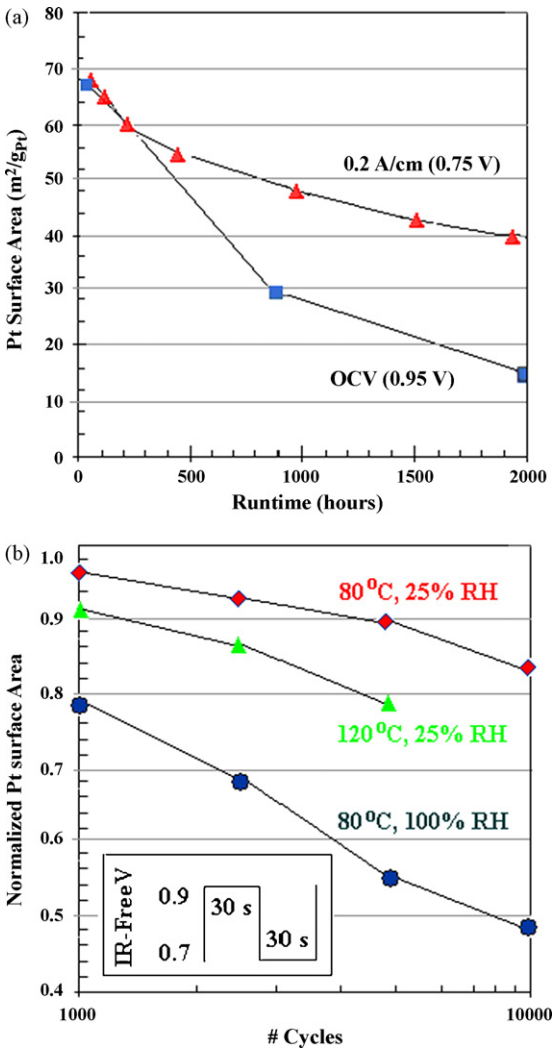

Fig. 2. Impact of operational conditions on catalyst active surface area loss. (a) Pt surface area as a function of stack runtime; (b) impact of RH and high temperature operation on Pt surface area loss of Pt/C as a function of potential cycles. (From [85] with permission.)

as shown in Fig. 2. However, carbon corrosion of the catalyst layer was recently found by Borup et al. [87] to increase with decreasing RH. They also revealed that the growth in cathode Pt particle size was much greater during potential cycling experiments than during steady state testing, and that it increased with an increase of potential, which was recently employed as an AST method to evaluate electrocatalyst stability.

Secondly, corrosion of the carbon support due to fuel starvation can be alleviated by enhancing water retention on the anode, such as through modifications to the PTFE and/or ionomer, the addition of water-blocking components like graphite, and the use of improved preferable catalysts for water electrolysis, as demonstrated by Knights et al. [6] in Fig. 3. With respect to PEM fuel cell freeze and rapid startup issues, two main strategies have been proposed to mitigate fuel cell performance degradation, based on whether the system uses extra energy during parking or startup. The first solution, the "keep-warm" method [88–90], is to consume power from a continuous or intermittent low-power energy source (from an extra battery or hydrogen fuel converter) to keep the system above a certain threshold temperature during the parking period. The other option is to heat the fuel cell system to raise its temperature above the freezing point of water at startup [91,92].

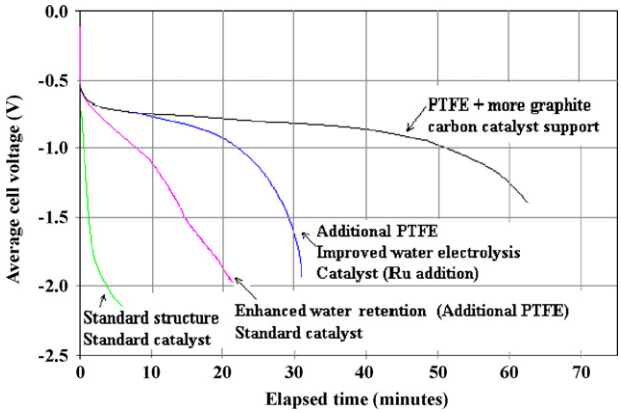

Fig. 3. Comparison of different anode structures in severe failure testing. Each cell has an equivalent cathode (~0.7 mg cm^{-2} Pt, supported on carbon). Testing conducted at 200 mg cm^{-2}, fully humidified nitrogen on anode. Anode loading at ~0.3 mg cm^{-2} Pt supported on carbon (varied materials and compositions). (Modified from [6] with permission.)

For this method, a higher power heat is required and it is strongly suggested that the method be combined with effective removal of residual water to save energy and alleviate physical damage to the MEA due to ice expansion. Possible methods for getting rid of the water include gas purging [6] or washing it away with an antifreeze solution [23] prior to fuel cell shutdown.

Thirdly, Pt-alloy catalysts such as PtCo, Pt–Cr–Ni have shown better activity and stability compared to pure Pt catalysts [93]. The increased sintering resistance offered by the alloying elements [93] or the larger alloy particle size [94] may explain the observed improvement. However, X-ray diffraction (XRD) analysis has revealed a skin consisting of a monolayer of pure Pt formed on the surface of the alloys after long-term testing [95–97]. This indicates that the non-noble metals in the Pt-transition metal alloy catalysts are more susceptible to dissolving in the ionomer phase, partially counteracting the advantage of Pt-alloy catalysts. Metals such as Co, Cr, Fe, Ni, and V have already proved to be soluble in a fuel cell operating environment; Pt–Co/C has drawn more attention recently due to its superior stability compared to that of the other Pt-transition alloy catalysts [94,98]. It is noteworthy that recently Adzic and co-workers [99] significantly improved the Pt stability against dissolution under potential cycling regimes by modifying Pt nanoparticles with gold (Au) clusters. There were no obvious changes in the activity and surface area of Au-modified Pt under oxidizing conditions and potential cycling between 0.6 and 1.1 V after over 30,000 cycles. The considerable improvement in the Au/Pt/C catalyst stability was mainly attributed to the existence of the non-dissolvable Au clusters. By strengthening the interaction between the metal particles and the carbon support, sintering and dissolution of the metal alloy catalysts can be alleviated. For example, Roy et al. [100] introduced nitrogen-based carbon functionality to the carbon support surface by chemical modification and, consequently, the ability of the treated support to anchor metal particles as well as its catalyst activity showed obvious improvement. Multiwalled carbon nanotubes (CNTs) have also demonstrated promise as catalyst supports in PEM fuel cell applications [101]. In a recent publication, Shao et al. [102] reported that the degradation rate of Pt/CNTs was nearly two times lower than that of Pt/C under the same accelerated durability testing conditions, which was attributed to the specific interaction between Pt and CNTs and to the higher resistance of the CNTs to electrochemical oxidation. In addition, the decrease in support surface area or graphitization of the carbon support can also enhance the support's resistance to oxidation and carbon corrosion [103,104]. However, the number of active surface sites on which to anchor metal particles correspondingly decreases, which is a potential detriment to the deposition of metal on the carbon support.

3.3. Gas diffusion layer

3.3.1. Gas diffusion layer degradation mechanisms

The gas diffusion layer (GDL) is typically a dual-layer carbon-based porous material, including a macroporous carbon fiber paper or carbon cloth substrate covered by a thinner microporous layer (MPL) consisting of carbon black powder and a hydrophobic agent. In past studies of GDLs, the impact of GDL materials and design on PEM fuel cell performance, rather than durability, has been the focal point. However, increased GDL surface hydrophilicity has been clearly observed after 11,000 h of operation [12] and cold start conditions [24], which unquestionably indicates that further investigation of the GDL is warranted. To date, only a limited number of studies have focused on the degradation mechanisms of GDLs or on the relationship between GDL properties and fuel cell performance decay. Moreover, these studies have employed mainly ex situ GDL aging procedures in order to avoid the possible confounding effects from adjoining components such as the catalyst layer and bipolar plate.

The results of Borup et al. [105] showed that the loss of GDL hydrophobicity increased with operating temperature and when sparging air was used instead of nitrogen. Additionally, they concluded that changes in the GDL properties were attributed mostly to the MPL. Frisk et al. [106] aged GDLs by submerging the samples in 15 wt.% hydrogen peroxide at 82 °C. They found that weight loss and the MPL contact angle increased with the time of exposure and the increase was attributed to oxidation of the carbon in the MPL. Kangasniemi et al. [107] demonstrated the effect of electrochemical surface oxidation on GDL properties and found that the contact angle of the MPL surface decreased remarkably over time when the GDL samples were immersed in 1 M H_2SO_4 under potentiostatic treatment of 1.2 V vs. standard hydrogen electrode (SHE). Most recently, Lee and Mérida [108] comprehensively studied GDL properties, such as electrical resistivity, bending stiffness, air permeability, surface contact angle, porosity, and water vapor diffusion, after degradation tests under steady state (over 1500 h aging time at 80 °C and 200 psi) and freezing (54 freeze-thaw cycles between −35 and 20 °C) conditions. As the fuel cell operates, the PTFE and carbon composite of the GDLs are susceptible to chemical attack (i.e., OH• radical as electrochemical byproduct) and electrochemical (voltage) oxidation [106]. The loss of PTFE and carbon results in the changes in GDL physical properties, such as the decrease of GDL conductivity and hydrophobicity, which further lowers MEA performance and negatively affects the durability of the whole fuel cell. With regard to the quantitative correlation between performance loss and the changes in GDL properties, Schulze et al. [109] recently found that the decomposition of PTFE in the electrodes induced an approximately two times higher performance loss than that related to the agglomeration of the platinum catalyst after 1000 h of fuel cell operation. However, the effect of PTFE degradation in the catalyst layer and GDL was not separated in their paper and the decomposition mechanism of PTFE was not thoroughly discussed.

3.3.2. Mitigation strategies for GDL degradation

Little information about mitigating GDL degradation is available from the literature. To improve GDL oxidative and electrooxidative stability, Borup [110] suggested using graphitized fibers during GDL preparation. Borup also proposed that higher PTFE loading could benefit the water management ability of aged GDLs, as shown in Fig. 4. By incorporating graphitized carbon material Pureblack®

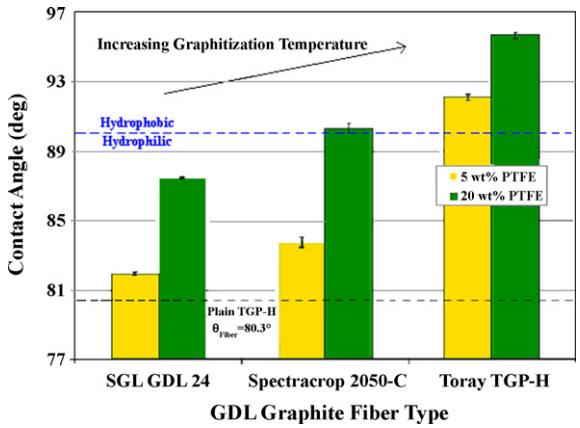

Fig. 4. Effect of GDL graphite fiber type and PTFE loading on contact angle. (Modified from [110] with permission.)

in the MPL, Owejan et al. [30] found a 25% improvement in the start/stop degradation rate at 1.2 A cm^{-2}.

3.4. Bipolar plate

3.4.1. Bipolar plate degradation mechanisms

The bipolar plate is a multifunctional component of the fuel cell stack, acting as a separator between the fuel, oxidant gases, and coolant; homogeneously distributing reactant and product streams; and collecting the current generated by the electrochemical reaction. A great deal of research and some literature reviews [111–114] related to bipolar plate studies have been published.

To fulfill all of the required functions, multiple properties are required for the materials to be acceptable for bipolar plates. These include, but are not limited to, high electrical conductivity, low gas permeability, high corrosion resistance, sufficient strength, low thermal resistance, and low cost, etc. In addition to graphite, materials such as metals, graphite/carbon-based composites, and polymer-based composites with conductive graphite/carbon fillers are currently being tested and evaluated by researchers [115–117]. The combination of high corrosion and chemical resistance, low density, and high electrical and thermal conductivity are attractive characteristics of graphite and graphite composites. However their durability under shock and vibration, permeability to hydrogen, and manufacturability are unfavorable when compared to metals, such that an increase in weight as well as volume is needed to overcome their shortcomings. Noble metals such as Pt, Ta, Nb, and Zr are highly corrosion resistant and are manufacturable as lightweight thin plates, but the raw material costs for these plates prohibit them from commercial applications [118]. As for other metallic bipolar plates, commercially available metals and their alloys such as Al, Ti, and Ni have exhibited inspiring potential in bipolar plates owing to their good electrical conductivity, excellent mechanical properties, and low cost. However, the major concern with these metallic bipolar plates is the contact resistance between the bipolar plate and the GDL, attributed to electrically resistant oxide films formed on the surfaces, which inevitably increase the internal electrical resistance of the fuel cell. Stainless steel has received considerable attention due to its wide range of alloy choices and applicability to mass production, but it is prone to corrosion in the aggressive acidic and humid environment inside a PEM fuel cell [119], which causes a further increase in contact resistance. Moreover, corrosion of metallic materials leads to the production of multivalent cations, which can seriously impair the durability of the membrane and catalyst [115], as discussed in Section 3.1.1. A chemical analysis of the MEA after 100 h of cell operation revealed that a large quantity of Fe and Ni atoms, as well as traces of Cr, was released from untreated stainless steel 316L [120]. As a result, a voltage drop of up to 300 mV at a current of 700 mA cm^{-2} was measured due to the chemical corrosion of this bipolar plate material. By exposing eight commercial stainless steels to an acid solution, Shores et al. [121] carried out an ex situ experiment to study the corrosion of stainless steel. A controlled potential was applied and the gas (H_2 or air) was bubbled into the solution to simulate either anode or cathode conditions. After 72 h of aging, the dissolved metal cations (including Fe^{+3}, Cr^{+3}, Ni^{+2}) were detected in the solution [121].

3.4.2. Mitigation strategies for bipolar plate degradation

Current work in this key area is focused mainly on the use of graphite/polymer composites, metallic materials coated with noble metals, or various nitride- or carbide-based alloys to improve corrosion resistance in real or simulated PEM fuel cell environments [122]. The most up-to-date research on carbon-based and metal-based coatings for PEM fuel cell bipolar plates, in addition to the corresponding coating techniques, are compiled in Table 3. Various coating methods that have been developed and applied widely in other industrial areas, such as immersion coating, spraying, electroplating, electroless deposition, electrolytic anodization, and painting [115], are being evaluated for bipolar plate materials. Taking cost competitiveness for continuous high-volume production into consideration, research in recent years [115] has focused on physical vapor deposition (PVD) and chemical vapor deposition (CVD) processes, as illustrated in detail in Table 3.

However, a potential risk with protective coating methods is the deformation of the coating material when the PEM fuel cell operates under thermal cycling conditions. Woodman et al. [148] proposed a reasonable explanation that the coating material and the substrate might expand and contract at different rates due to the difference in their coefficients of thermal expansion (CTEs). The micro-pores and micro-cracks arising from deformation of the coating layer can lead to the direct exposure of the substrate metal to a highly corrosive environment and, subsequently, the dissolved metal ions diffuse into the membrane and get trapped in the ion exchange sites, resulting in considerable adverse effects on cell performance. The addition of intermediate coating layers with high bonding strength and gradient CTEs between adjacent layers of the coating and bipolar plate is one effective strategy for buffering the CTE differential.

Another common concern related to bipolar plates is the possible deformation or even fracture caused by the compressive forces that are used to ensure good electric contact and reactant sealing during fuel cell operation [149]. Some operational factors, such as thermal cycling, non-uniform current, or thermal misdistributions over the active area, can impair the mechanical properties of the bipolar plate materials. Hodgson and Farndon [150] and Lee et al. [151] subjected the surface of a metallic material, such as stainless steel or nickel-rich alloys, to an electrical current in the presence of an acidic electrolyte. After this treatment, the corrosion resistance of the metallic bipolar plate was improved, which was attributed to the modification of the surface composition and/or the surface morphology. This surface treatment method is particularly promising since the treatment is a modification to the surface rather than a coating procedure and therefore delamination is not an issue.

Table 4 presents research on composite bipolar plate materials, including carbon–polymer composites and carbon–carbon composites, with a summary of their advantages and disadvantages. As shown, carbon–carbon composites have many advantages, although their lack of mechanical strength in addition to the lengthy and expensive chemical vapor impregnation (CVI) process destines them to limited success. Recently, carbon–polymer materials, especially those with thermoset resins, are becoming competitive

Table 3
Practicable coated metallic bipolar plates proposed in the literature

Coating category	Coating method	Coating materials	Applicable base plate materials				Reference
			Al	Ti	Ni	Other	
Metal-based coating							
Noble metals	Pulse current electrodeposition	Gold over Ni over Cu	X				[123,124]
	Electrodeposition	Gold	X			Stainless steel (SS)	[125]
	DC magnetron sputtering	Ta	X			SS316	[120]
	Electroplating	Gold			X		[120]
Metal nitrides	PVD (e.g. magnetron sputtering) or CVD, and electrolessdeposition for Ni-Ph alloy	(1) Sublayer-Cr/Ni/Mo-rich SS or Ni-phosphorus alloy; (2) topcoat-Ti nitride	X	X		SS	[126]
	Radio frequency (RF)-planar magnetron (sputtering)	Ti–Al–nitride layer	X				[127]
	RF-diode sputtering	TiN layer		X			[127]
	Thermal nitridation	CrN/Cr_2N surface				Cr-bearing alloy	[128–132]
						Ferritic SS	[133,134]
						Austenitic SS	[132,135]
	PVD	NS				SS304	[136]
	PVD	TiN				SS410	[137]
	Electrodeposition	TiN				SS316	[138]
	NS	TiN				SS316	[121]
Metal carbides	Glow discharge decomposition and vapor deposition	(1) n-Type silicon carbide (SiC); (2) gold				SS	[127]
	Electro-spark deposition process	Cr carbide				SS310	[139]
Metal oxide	Electron beam evaporation	Indium doped tin oxide ($Sn(In)O_2$)		X			[127]
	Vapor deposition and sputtering	(1) Sublayer-lead; (2) topcoat-lead oxide (PbO/PbO_2)		X			[127]
Carbon-based coating							
Graphite	Painting or pressing	(1) Sublayer-sonicated graphite particles in an emulsion, suspension or paint (e.g. graphite particles in an epoxy resin thinned by an organic solvent, such as toluene); (2) topcoat-exfoliated graphite in the form of sheets of flexible, graphite foil	X	X	X		[140]
	PVD (closed-field, unbalanced, magnetron sputter ion plating) and chemical anodization/oxidation overcoating	(1) Sublayer-titanium over titanium-aluminum-nitride; (2a) overcoat-transient metal sublayer of Cr (Ti, Ni, Fe, Co) followed by sulphuric/chromic acid OR; (2b) topcoat-graphite	X	X	X	SS	[140]
Conductive polymer	NS	Organic self-assembled monopolymers	NS				[141]
	NS	Conductive polymers	NS				[141]
	Electrodeposition	Conductive polymers polyaniline (PANI) and polypyrrole (PPY)				SS304	[142]
	Plasma-polymer coating	Hexafluoropropylene (HFP)		X		SS304	[143]
	Electrodeposition	Multilayer coating (Ni, Au) conductive polymer (polyaniline)	X				[123]
	Spraying	(1) Sublay-conductive polymer (M2-48); (2) interlay- commercial graphite (TV-Koat); (3) topcoat-conductive polymer (M2-48)				SS316L	[144]
	NS	Coating comprised of carbon fibers contained within a polymer matrix				SS	[145]
Diamond or diamond-like carbon	NS	Diamond-like carbon	NS				[141]
	PVD	YZU001 diamond-like material	X			SS316	[146]
Organic self-assembled monoploymers	NS	Organic self-assembled monopolymers	NS				[147]

Note: Not specified (NS).

alternatives to bipolar plates in terms of bulk conductivity and dimensional tolerance. However, high carbon loadings are always necessary to obtain the required electrical conductivity, which eventually causes difficulties in processability. Another problem associated with carbon–polymer materials is the degradation of the resins in PEM fuel cell working environments due to the inherent properties of these polymers [111]. The heavy atoms released from these resins as a consequence, such as calcium, magnesium, or zinc, may diffuse into and contaminate the PEM, decreasing fuel cell durability.

Following principles of stack manufacturing and environmental impact, Cooper has identified 51 bipolar plate requirements and

Table 4
Practicable carbon composite bipolar plates proposed in the literature

Carbon composite	Polymer	Filler	Fiber	Reference	Advantages	Disadvantages
Carbon–polymer composite						
Thermoplastic	PVDF	Carbon/graphite particles		[152]	Injection molding lends itself to manufacturing automation	Low electrical conductivity when using standard thermoplastics
	PVDF	Carbon/graphite particles	Carbon/graphite fibers	[153]	Fast cycle time	Limited to low-temperature operation
	PVDF	Carbon black, graphite powder	Carbon/graphite fibers	[154]	Flow field introduced during molding	Injection molding difficult at high carbon loading
	PVDF	Carbon black		[155]	Low contact resistance	Generally less chemically stable than thermoset resins
	Liquid crystal polymer (LCP)	Carbon black	Carbon fibers	[156]		Difficult to increase carbon concentration
	Polyethylene terephthalate (PET)/PVDF	Carbon or CNT		[157]		
Thermoset	Mixture of epoxy resin and aromatic amine hardener	Graphite powder		[158]	Higher temperature operation than thermoplastic	Relatively low electrical conductivity
	Phenyl-aldehyde resol or novolac	Graphite powder	Graphite fibers	[159]	Flow field introduced during molding	Difficult to increase carbon concentration
	Phenyl-aldehyde resol or novolac	Coke-graphite particles		[160]	Low contact resistance	
	Reichhold 24-655 phenolic resin	Graphite powder	Cellulose fibers (not rayon or cellulose acetate)	[161]		
	Furan resin or phenolic resin	Graphite powder	Cellulose fibers (not rayon or cellulose acetate)	[162]		
	Vinyl ester	Graphite powder		[163,164]		
Carbon–carbon composites						
	Phenolic resin	Carbon fiber	Vapor-infiltrated carbon	[165,166]	High electrical conductivity	Long and expensive CVI process is necessary to deposit graphitic carbon and to pyrolize resins (bulk processing and automation set to lower price)
	Unsaturated polymer	Compound graphite powder		[167]	High thermal conductivity	Lack of mechanical strength
	Epoxy resin	Pan-based carbon fiber	Vapor-infiltrated carbon	[168]	Lightweight	
	Phenol-formaldehyde resin	Pan-based carbon fiber, carbon black	Vapor-infiltrated carbon	[169]	High temperature operation High strength Highly corrosion and chemical resistance Flow field introduced during stamping of perform	

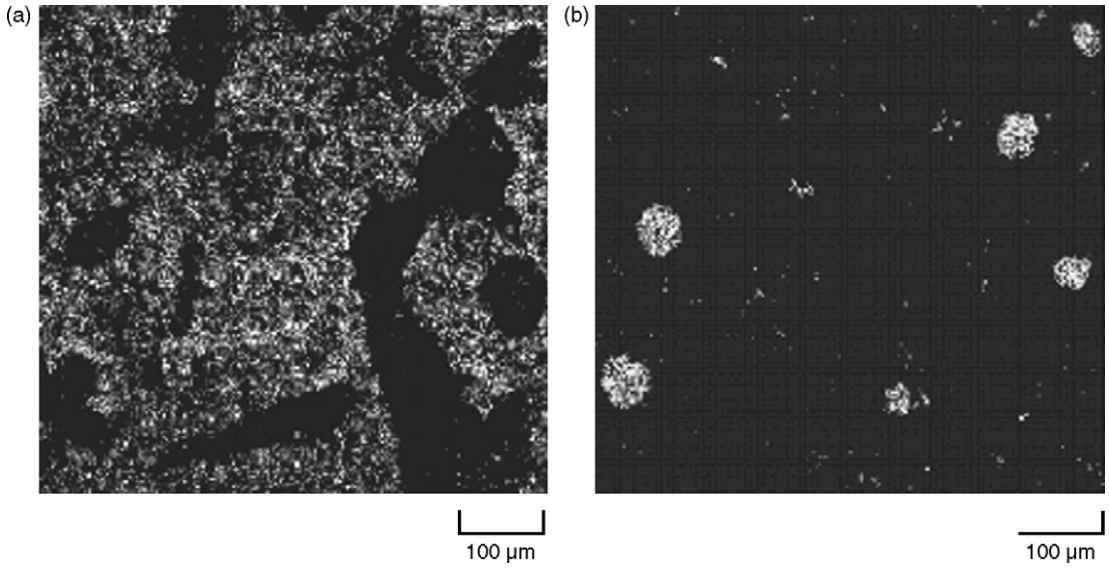

Fig. 5. SEM–EDX images of an embrittled membrane sample. The holes and tears resulted from reduced mechanical integrity caused by the crystallization of (a) silicon- and (b) calcium-containing particles from the degradation of incompatible sealing materials inside and on the surface of a membrane. (From [174] with permission.)

design rules for PEM fuel cells [170]. Among the state-of-the-art alternatives for bipolar plates, although no material has definitely established itself as capable of meeting all the desired target properties for commercial applications [131], each material has its specific advantages and disadvantages and, therefore, will find its specific application fields. The choice of material depends on the driving constraints of the application and is always a compromise between performance, efficiency, size, lifetime, cost, operational range flexibility, local climate, and so on.

3.5. Sealing gasket

Sealing material is placed between the bipolar plates to prevent gas and coolant leakage and crossover. Typical sealing materials utilized in PEM fuel cells include fluorine caoutchouc, EPDM, and silicone [171]. Tan et al. [172] reported their results from a recent ex situ investigation on the chemical degradation of four commercial gasket materials in simulated fuel cell environments. Cleghorn et al. [4] and St-Pierre and Jia [12] observed the degradation and dissolution of silicone in the active section of the stack during their lifetime experiments. Schulze et al. [171] detailed the degradation of silicon-based seals during long-term fuel cell operation. They detected residues of the silicone in the anode catalyst layer and cathode GDL by XPS. The authors concluded that the direction of movement of the silicone traces was from the anode to the cathode due to the electrical field and that it was blocked by the PEM. However, traces of decomposition products of the sealing material in both the membrane and electrodes, as shown in Fig. 5, have been detected by Ahn et al. [14], Xie et al. [173], and Du et al. [174]. The acid character of the PEM, together with the thermal stressing [171] or hydrogen embrittlement [12], possibly induces the alteration of the sealing material. The degradation of the seals results in the loss of their force retention and can lead to compression loss, external leaks of coolant, gas crossover, or plate electrical shorting, eventually accelerating the performance degradation of the fuel cell. The migration and accumulation of the sealing materials within the electrodes will also negatively change the hydrophobic character of the electrodes and probably poison the Pt catalysts. Furthermore, the traces from the seal may diffuse into the membrane phase and consequently lead to a decrease in membrane conductivity and a reduction in the mechanical integrity of the membrane, both of which would severely impair the fuel cell lifetime [174]. Seal selection through ex situ and in situ screening processes should be based on the overall chemical and mechanical properties of the

Table 5
Major failure modes of different components in PEM fuel cells [3,175]

Component	Failure modes	Causes
Membrane	Mechanical degradation	Mechanical stress due to non-uniform press pressure, inadequate humidification or penetration of the catalyst and seal material traces
	Thermal degradation	Thermal stress; thermal cycles
	Chemical/electrochemical degradation	Contamination; radical attack
Catalyst/catalyst layer	Loss of activation	Sintering or dealloying of electrocatalyst
	Conductivity loss	Corrosion of electrocatalyst support
	Decrease in mass transport rate of reactants	Mechanical stress
	Loss of reformate tolerance	Contamination
	Decrease in water management ability	Change in hydrophobicity of materials due to Nafion or PTFE dissolution
GDL	Decrease in mass transport	Degradation of backing material
	Decrease in water management ability	Mechanical stress; Change in the hydrophobicity of materials
	Conductivity loss	corrosion
Bipolar plate	Conductivity loss	Corrosion; oxidation
	Fracture/deformation	Mechanical stress
Sealing gasket	Mechanical failure	Corrosion; mechanical stress

Table 6
General AST methods in PEM fuel cell lifetime analysis

Component	General criteria	Failure modes	Available protocols	Reference
Membrane/MEA	OCV at reduced RH for chemical stability; RH cycling for mechanical degradation	Chemical stability	Fenton's test: 30% H_2O_2, 20 ppm Fe^{+2}, 85 °C, 3 cycles with fresh reagent	[176]
		Chemical/electrochemical stability	OCV, 90 °C, with partially humidified H_2 and O_2 (both 30% RH) introduced to anode and cathode, respectively	[37]
			OCV, 80 °C, with dry air and fully humidified H_2 supplied to cathode and anode, respectively	[36]
			OCV, 90 °C, with partially humidified H_2 and air (both 30% RH) introduced to anode and cathode, respectively	[177]
			OCV, 95 °C, with partially humidified H_2 and air (both 50% RH) introduced to anode and cathode, respectively	[82]
			OCV, 90 °C, with partially humidified H_2 and O_2 (both 30% RH) introduced to anode and cathode, respectively	[178]
		Mechanical stability	65 °C, RH cycling from 30 to 80% or from 80 to 120% with 30 min/step, with air supplied to anode and cathode	[37]
			80 °C, RH cycling from 0 to 150% with 2 min/step, with air supplied to anode and cathode sides	[85]
		Chemical and mechanical stability	Humidity cycle: N_2/N_2, 80 °C, RH of inlet gases cycled between 0 and 100% RH every 30 min	[178]
			Load cycle: H_2/O_2, 50% RH, 80 °C, load cycled between 10 and 800 mA cm^{-2} (7 min/3 min)	[178]
Catalyst/catalyst layer	Potential cycling; acid washing; elevated temperatures; fuel or oxidant contaminants	Pt and/or Pt alloy chemical and electrochemical stability	80 °C, 100% RH, step change (30 s/step) in voltage from 0.6 to 0.96 V with air on cathode and H_2 on anode	[178]
			80 °C, 100% RH, 20 mV s^{-1}, linear sweep in voltage from 0.6 to 1.2 V with N_2 on cathode and H_2 on anode	[178]
			60 or 80 °C, 50% or 100% RH, with N_2 on cathode and H_2 on anode, 10 mV s^{-1}, from 0.1 to either 1.0 or 1.2 V	[179]
			80 °C, 100% RH, cathode 1.2 V relative to anode, with N_2 on cathode and H_2 on anode	[106]
			80 °C, H_2 with 226% RH at anode, Air with 100% RH at cathode, 10 mV s^{-1} potential cycling from 0.1 to 1.2 V	[110]
			80 °C, 100% RH, step change (30 s/step) in voltage from 0.6 to 0.9 V with N_2 on cathode and H_2 on anode	[177]
			20 °C, 0.5 M H_2SO_4, potentiostatic treatment 1.2 V (vs. RHE)	[102]
			40 or 80 °C, 1 M $HClO_4$, potential cycling between 0.85 V (vs. RHE) and 1.4 V (vs. RHE)	[180]
		Carbon support stability	80 °C, 100% RH, Potential hold at 1.2 V, with N_2 on cathode and H_2 on anode	[181]
			80 °C, 100% RH, Potential hold at 1.5 V, with N_2 on cathode and H_2 on anode	[181]
			OCV, 80 °C, with partially humidified H_2 and air (both 66% RH) introduced to anode and cathode, start/stop cycles between H_2/air (45/100 sccm) for 30 s and air/air (45/0 sccm) for 20 s.	[84]
			50 °C, with fully humidified 4% H_2/N_2 and He for anode and cathode respectively, 2 mV s^{-1} potential cycling between 0.04 V (vs. RHE) and 1.2 V (vs. RHE)	[84]
			95 °C, 80% RH, potential hold at 1.2 V, with N_2 on cathode and H_2 on anode	[177]
GDL	Chemical oxidation in hydrogen peroxide (H_2O_2); elevated potential; low humidity	Chemical/electrochemcial oxidation	DI water, 60 or 80 °C, purged with N_2 or air	[105]
			15 wt.% H_2O_2 at 82 °C	[106]
			1 M H_2SO_4, under potentiostatic treatment of 1.2 V (vs. RHE)	[107]
			80 °C, with fully humidified H_2 and N_2 for anode and cathode respectively, 1.2 V (vs. RHE)	[30]
		Mechanical stability	Compressive stress at 80 °C and 200 psi	[108]
			Freeze-thaw cycles between −35 and 20 °C	[108]

Table 6 (*Continued*)

Component	General criteria	Failure modes	Available protocols	Reference
Bipolar plates	Press-stress; acid treatment; load cycling; temperature cycling	Chemical/electrochemical stability	1 M H_2SO_4 + 2 ppm F^-, 70 °C, linear sweep: −0.5 to 1.2 V or potentiostatic polarization: 0.1 V vs. normal hydrogen electrode (NHE) for anode and 0.8 V (vs. NHE) for cathode, purged with H_2 for anode and air for cathode	[131–137]
			0.01 M HCl + 0.01 M Na_2SO_4, 80 °C, linear sweep: −0.5 to 1.0 V or potentiostatic polarization: −0.24 V vs. saturated calomel electrode (SCE) for anode and 0.6 V (vs. SCE) for cathode, purged with H_2 for anode and O_2 for cathode	[138]
			0.1 M HCl, linear sweep: 0 V (vs. RHE) to 1.0 V (vs. RHE)	[182]
			0.1 M K_2SO_4, pH 1, 80 °C, linear sweep: −0.5 to 1.2 V or potentiostatic polarization: 0.0 V for anode and 0.6 V (vs. NHE) for cathode, Purged with H_2 for anode and air for cathode	[121]
			H_2SO_4 and Na_2SO_4, pH 4.8, linear polarization: −1.5 to 1.5 V (vs. SCE), room temperature, no reactant gas	[183]
			0.5 M H_2SO_4, linear polarization: −0.5 to 0.5 V (vs. OCV), room temperature, purged with air	[129,151,184,185]
			0.001N H_2SO_4 + 2 ppm F^-, 80 °C, potentiostatic polarization: 1.0 V (vs. NHE), purged with N_2	[165]
			0.001 M H_2SO_4 + 0.00015 M HCl + 15 ppm HF, 70 °C, linear polarization: −0.309 to 0.941 V (vs. NHE), purged with H_2 for anode and O_2 for cathode	[119]
Sealing gasket	Temperature; acid treatment; deformation/press-stress	Chemical and mechanical stability	Bend strip environmental stress crack resistance tests with various bend angles, 1 M H_2SO_4 + 10 ppm HF	[172]
		Chemical stability	0.35 M acid 1 + 10 ppm acid 2 + 3 wt.% H_2O_2	[174]

materials [172]. With regard to seal material degradation, no available publications relevant to mitigation strategies have yet been found.

In summary, the major failure modes for PEM fuel cell components, including the membrane, catalyst/catalyst layer, GDL, bipolar plate, and sealing material, are listed in detail in Table 5.

4. Accelerated stress test methods and protocols

The traditional durability data analysis in engineering involves analyzing times-to-failure data obtained under normal operating conditions in order to quantify the life characteristics of the product, system, or component. In the case of fuel cells, such times-to-failure data are always very difficult to obtain due to the issues mentioned above: prolonged test periods and high costs. More importantly, a fuel cell stack is a complicated system comprising various components for which the degradation mechanisms, component interactions, and effects of operating conditions need to be fully understood prior to establishing fuel cell commercial viability. As mentioned above, several fuel cell developers have implemented various ASTs to analyze failure modes of current fuel cell components, in order to increase sample throughput and reduce experimental time. Currently, the DOE and the US Fuel Cell Council (USFCC) are each trying to establish PEM fuel cell durability testing protocols with the intent to provide a standard set of test conditions and operating procedures for evaluating new cell component materials and structures. ASTs published in the available literature other than the DOE and USFCC protocols are categorized in Table 6. An accelerated stress testing method should not only activate the targeted failure mode of the specific component, but it should also minimize the confounding effects from other components. For instance, the AST protocol for catalyst supports is different from that of the electrocatalyst because the components experience different degradation mechanisms under different conditions. Similarly, the AST for the mechanical degradation of the membrane should distinguish and isolate the effects of the chemical degradation of the membrane.

5. Conclusions

At present, durability, cost, and reliability are delaying the commercialization of PEM fuel cell technology. Above all, durability is the most critical issue and influences the other two issues. Various efforts have been made to investigate the degradation mechanisms of fuel cell systems and components in an attempt to enhance the durability of fuel cells. However, the current understanding of the degradation mechanisms of PEM fuel cell components is still insufficient. To this end, more emphasis needs to be placed on innovative diagnostic methods and analytical instruments. Moreover, there is a lack of information about the quantitative correlations between the degradation of individual components within the fuel cell and the resulting performance loss. Continuing efforts are critical to propose necessary mitigation strategies and eventually to facilitate the move toward commercialization of PEM fuel cell technology.

With respect to membrane durability, great achievements have been made by modifying the membrane structure to improve its chemical/electrochemical stability and by using a PTFE-reinforced membrane to enhance its mechanical stability. However, further improvements in preventing crossover and preserving stability are necessary for successful operation in the rugged environment of automotive applications rather than only under mild steady state conditions.

Similarly, catalysts must also survive the harsh transient operations of a vehicle, such as load and RH cycles. Unfortunately, the

catalyst decay that occurs with current materials is still too high to meet DOE performance targets. Further optimization of materials and an improved understanding of degradation mechanisms are needed to alleviate Pt dissolution and carbon corrosion. Pt-alloy catalysts, such as Pt–Co, Pt–Au, or Pt–Cr–Ni, loaded on supports with a high resistance to electrochemical oxidation, are suggested for further work.

As for the bipolar plate material, there has been significant ongoing research on both coated metal plates and carbon/graphite composites. Further improvement in the corrosion resistance of metallic materials is necessary prior to their widespread use. In addition to various coating methods, innovative treatments of the metal surface such as electrochemical treating and a thermal nitridation approach show promise for avoiding the possible delamination between the base metal and the protective coating due to different CTEs. On the other hand, carbon–polymer composites, especially carbon/thermoset resins composites, are becoming competitive alternatives to bipolar plate material by virtues of their high bulk conductivity and dimensional tolerance. Once measures are taken to mitigate their property shortcomings such as gas permeability, the remaining barrier will still be the cost.

The limited research on GDLs and sealing materials is based mainly on ex situ analysis. Accelerated stresses include mechanical press and/or chemical oxidation. More work in these areas is needed to improve fuel cell stability in the long term.

The establishment of AST protocols will provide a standard set of test conditions and operating procedures for evaluating new cell component materials and structures. The present AST protocols developed individually by DOE and USFCC are still limited to the component level (electrocatalyst, catalyst support, membrane, and MEA). It is worthwhile to note that, even though these two protocols generally agree with each other, they are still different in a few areas. The completion and unanimity of AST protocols for the PEM fuel cell as a whole, in addition to those for the components, are imperative in the near future.

Acknowledgments

The authors gratefully acknowledge the National Fuel Cell program of the National Research Council of Canada (NRC) and the NRC–Helmholtz cooperative research program for supporting this project.

References

[1] http://www.fossil.energy.gov/programs/powersystems/fuelcells/ (accessed December 2007).
[2] D.P. Wilkinson, J. St-Pierre, in: W. Vielstich, H.A. Gasteiger, A. Lamm (Eds.), Handbook of Fuel Cells: Fundamentals, Technology and Applications, vol. 3, John Wiley & Sons Ltd., 2003, pp. 611–626.
[3] M. Fowler, R.F. Mann, J.C. Amphlett, B.A. Peppley, P.R. Roberge, in: W. Vielstich, H.A. Gasteiger, A. Lamm (Eds.), Handbook of Fuel Cells: Fundamentals, Technology and Applications, vol. 3, John Wiley & Sons Ltd., 2003, pp. 663–677.
[4] S.J.C. Cleghorn, D.K. Mayfield, D.A. Moore, J.C. Moore, G. Rusch, T.W. Sherman, N.T. Sisofo, U. Beuscher, J. Power Sources 158 (2006) 446–454.
[5] S. Srinivasan, B. Kirby, in: S. Srinivasan (Ed.), Fuel Cells: From Fundamentals to Applications, Springer Science/Business Media, 2006, pp. 542–552.
[6] S.D. Knights, K.M. Colbow, J. St-Pierre, D.P. Wilkinson, J. Power Sources 127 (2004) 127–134.
[7] T. Ralph, Platinum Met. Rev. 41 (1997) 102–113.
[8] J. St-Pierre, D.P. Wilkinson, S. Knights, M. Bos, J. New Mater. Electrochem. Syst. 3 (2000) 99–106.
[9] K. Washington, Proceedings of Fuel Cell Seminar 2000, Portland, USA, November, 2000, pp. 468–472.
[10] E. Endoh, S. Terazono, H. Widjaja, The Electrochem. Soc. 202nd Meeting Abstracts, Salt Lake City, USA, 2002 (abstract 89).
[11] O. Yamazaki, M. Echigo, T. Tabata, Proceedings of Fuel Cell Seminar 2002, Palm Springs, USA, November, 2002, pp. 105–108.
[12] J. St-Pierre, N. Jia, J. New Mater. Electrochem. Syst. 5 (2002) 263–271.
[13] M.W. Fowler, R.F. Mann, J.C. Amphlett, B.A. Peppley, P.R. Roberge, J. Power Sources 106 (2002) 274–283.
[14] S.Y. Ahn, S.J. Shih, H.Y. Ha, S.A. Hong, Y.C. Lee, T.W. Lim, I.H. Oh, J. Power Sources 106 (2002) 295–303.
[15] X. Cheng, L. Chen, C. Peng, Z. Chen, Y. Zhang, Q. Fan, J. Electrochem. Soc. 151 (2004) A48–A52.
[16] J. Scholta, N. Berg, P. Wilde, L. Jorissen, J. Garche, J. Power Sources 127 (2004) 206–212.
[17] C. Sishtla, G. Koncar, R. Platon, S. Gamburzev, J. Power Sources 71 (1998) 249–255.
[18] T. Nakayama, Proceedings of Fuel Cell Seminar 2000, Portland, USA, 2000, pp. 391–394.
[19] T. Isono, S. Suzuki, M. Kaneko, Y. Akiyama, Y. Miyake, I. Yonezu, J. Power Sources 86 (2000) 269–273.
[20] H. Meada, A. Yoshimura, H. Fukumoto, Proceedings of Fuel Cell Seminar 2000, Portland, USA, 2000, pp. 379–400.
[21] S. Sakamoto, A. Fuju, K. Shindo, S. Yoshida, S. Yoshida, K. Nakato, N. Nishizawa, Proceedings of Fuel Cell Seminar 2000, Portland, USA, 2000, pp. 85–94.
[22] M. Fowler, J.C. Amphlett, R.F. Mann, B.A. Peppley, P.R. Roberge, J. New Mater. Electrochem. Syst. 5 (2002) 255–262.
[23] E.A. Cho, J.J. Ko, H.Y. Ha, S.A. Hong, K.Y. Lee, T.W. Lim, I.H. Oh, J. Electrochem. Soc. 151 (2004) A661–A665.
[24] M. Oszcipok, D. Riemann, U. Kronenwett, M. Kreideweis, M. Zedda, J. Power Sources 145 (2005) 407–415.
[25] J. Xie, D.L. Wood III, D.M. Wayne, T.A. Zawodzinski, P. Atanassov, R.L. Borup, J. Electrochem. Soc. 152 (2005) A104–A113.
[26] J. Yu, T. Matsuura, Y. Yoshikawa, M.N. Islam, M. Hori, Electrochem. Solid-State Lett. 8 (2005) A156–A158.
[27] E. Endoh, H. Kawazoe, S. S Honmura, Proceedings of Fuel Cell Seminar 2006, Honolulu, Hawaii, USA, November, 2006, pp. 284–287.
[28] B. Du, R. Pollard, J. Elter, Proceedings of Fuel Cell Seminar 2006, Honolulu, Hawaii, USA, November, 2006, pp. 61–64.
[29] H. Xu, M. Wu, Y. Liu, V. Mittal, R. Vieth, H.R. Kunz, L.J. Bonville, J.M. Fenton, ECS Trans. 3 (2006) 561–568.
[30] J.E. Owejan, P.T. Yu, R. Makharia, ECS Trans. 11 (2007) 1049–1057.
[31] D. Dunwoody, J. Leddy, Electrochem. Soc. Interf. 14 (2005) 37–39.
[32] A. Collier, H. Wang, X. Yuan, J. Zhang, D.P. Wilkinson, Int. J. Hydrogen Energy 31 (2006) 1838–1854.
[33] A.B. LaConti, M. Hamdan, R.C. McDonald, in: W. Vielstich, H.A. Gasteiger, A. Lamm (Eds.), Handbook of Fuel Cells: Fundamentals Technology and Applications, vol. 3, John Wiley & Sons Ltd., 2003, pp. 647–662.
[34] F.N. Büchi, S. Srinivasan, J. Electrochem. Soc. 144 (1997) 2767–2772.
[35] J. Yu, T. Matsuura, Y. Yoshikawa, M.N. Islam, M. Hori, Phys. Chem. Chem. Phys. 7 (2005) 373–378.
[36] E. Endoh, S. Terazono, H. Widjaja, Y. Takimoto, Eletrochem. Solid-State Lett. 7 (2004) A209–A211.
[37] X. Huang, R. Solasi, Y. Zou, M. Feshler, K. Reifsnider, D. Condit, S. Burlatsky, T. Madden, J. Polym. Sci. 16 (2006) 2346–2357.
[38] C. Yang, S. Srinivasan, A.B. Bocarsly, S. Tulyani, J.B. Benziger, J. Membr. Sci. 237 (2004) 145–161.
[39] C. Ma, L. Zhang, S. Mukerjee, D. Ofer, B. Nair, J. Membr. Sci. 219 (2003) 123–136.
[40] C.A. Wilkie, J.R. Thomsen, M.L. Mittleman, J. Appl. Polym. Sci. 42 (1991) 901–909.
[41] J. Surowiec, R. Bogoczek, J. Therm. Anal. 33 (1988) 1097–1102.
[42] D. Chu, D. Gervasio, M. Razaq, E.B. Yeager, J. Appl. Electrochem. 20 (1990) 157–162.
[43] Q. Deng, C.A. Wilkie, R.B. Moore, K.A. Mauritz, Polymer 39 (1998) 5961–5972.
[44] S.R. Samms, S. Wasmus, R.F. Savinell, J. Electrochem. Soc. 143 (1996) 1498–1504.
[45] Y.S. Kim, L. Dong, M.A. Hickner, T.E. Glass, V. Webb, J.E. McGrath, Macromolecules 36 (2003) 6281–6285.
[46] M. Cappadonia, J.W. Erning, U. Stimming, J. Electroanal. Chem. 376 (1994) 189–193.
[47] N. Sivashinsky, G.B. Tanny, J. Appl. Polym. Sci. 26 (1981) 2625–2637.
[48] R.C. McDonald, C.K. Mittelsteadt, E.L. Thompson, Fuel Cells 4 (2004) 208–213.
[49] M. Inaba, T. Kinumoto, M. Kiriake, R. Umebayashi, A. Tasaka, Z. Ogumi, Electrochim. Acta 51 (2006) 5746–5753.
[50] X. Cheng, J. Zhang, Y. Tang, C. Song, J. Shen, D. Song, J. Zhang, J. Power Sources 167 (2007) 25–31.
[51] F.N. Büchi, B. Gupta, O. Haas, G.G. Scherer, Electrochim. Acta 40 (1995) 345–353.
[52] H. Wang, G.A. Capuano, J. Electrochem. Soc. 145 (1998) 780–784.
[53] C. Huang, K.S. Tan, J. Lin, K.L. Tan, Chem. Phys. Lett. 371 (2003) 80–85.
[54] G.G. Scherer, Phys. Chem. 94 (1990) 1008–1014.
[55] A. Pozio, R.F. Silva, M. De Francesco, L. Giorgi, Electrochim. Acta 48 (2003) 1543–1549.
[56] S. Stucki, G.G. Scherer, S. Schlagowski, E. Fischer, J. Appl. Electrochem. 28 (1998) 1041–1049.
[57] J.R. Yu, B.L. Yi, D.M. Xing, F.Q. Liu, Z.G. Shao, Y.Z. Fu, H.M. Zhang, Phys. Chem. Chem. Phys. 5 (2003) 611–615.
[58] B. Mattsson, H. Ericson, L.M. Torell, F. Sundholm, Electrochim. Acta 45 (2000) 1405–1408.
[59] X. Cheng, Z. Shi, N. Glass, L. Zhang, J. Zhang, D. Song, Z. Liu, H. Wang, J. Shen, J. Power Sources 165 (2007) 739–756.

[60] T. Okada, in: W. Vielstich, H.A. Gasteiger, A. Lamm (Eds.), Handbook of Fuel Cells: Fundamentals, Technology and Applications, vol. 3, John Wiley & Sons Ltd., 2003, pp. 628–646.
[61] R. Borup, J. Meyers, B. Pivovar, Y.S. Kim, R. Mukundan, N. Garland, D. Myers, M. Wilson, F. Garzon, D. Wood, P. Zelenay, K. More, K. Stroh, T. Zawodzinski, J. Boncella, J.E. McGrath, M. Inaba, K. Miyatake, M. Hori, K. Ota, Z. Ogumi, S. Miyata, A. Nishikata, Z. Siroma, Y. Uchimoto, K. Yasuda, K. Kimijima, N. Iwashita, Chem. Rev. 107 (2007) 3904–3951.
[62] D.E. Curtin, R.D. Lousenberg, T.J. Henry, P.C. Tangeman, M.E. Tisack, J. Power Sources 131 (2004) 41–48.
[63] W. Liu, K. Ruth, G. Rusch, J. New Mater. Electrochem. Syst. 4 (2001) 227–231.
[64] D.A. Shores, G.A. Deluga, in: W. Vielstich, H.A. Gasteiger, A. Lamm (Eds.), Handbook of Fuel Cells: Fundamentals Technology and Applications, vol. 3, John Wiley & Sons Ltd., 2003, pp. 273–285.
[65] W. Yan, S. Mei, C. Soong, Z. Liu, D. Song, J. Power Sources 160 (2006) 116–122.
[66] J.F. Wu, B.L. Yi, M. Hou, Z.J. Hou, H.M. Zhang, Eletrochem. Solid-State Lett. 7 (2004) A151–A154.
[67] M. Wakizoe, H. Murata, H. Takei, Proceedings of Fuel Cell Seminar 1998, Portland, USA, 1998, pp. 487–490.
[68] Q.F. Li, R.H. He, J.O. Jensen, N.J. Bjerrum, Chem. Mater. 15 (2003) 4896–4915.
[69] O. Savadogo, J. Power Sources 127 (2004) 135–161.
[70] G. Alberti, M. Casciola, Annu. Rev. Mater. Res. 33 (2003) 129–154.
[71] J.J. Zhang, Z. Xie, J.J. Zhang, Y.H. Tang, C.J. Song, T. Navessin, Z.Q. Shi, D.T. Song, H.J. Wang, D.P. Wilkinson, Z.S. Liu, S. Holdcroft, J. Power Source 160 (2006) 872–891.
[72] L. Gubler, H. Kuhn, T.J. Schmidt, G.G. Scherer, H.P. Brack, K. Simbeck, Fuel Cells 4 (2004) 196–207.
[73] L. Gubler, S.A. Gürsel, G.G. Scherer, Fuel Cells 5 (2005) 317–335.
[74] V. Ramani, H.R. Kunz, J.M. Fenton, J. Power Sources 152 (2005) 182–188.
[75] G.M. Haugen, F. Meng, N. Aieta, J.L. Horan, M.C. Kuo, M.H. Frey, S.J. Hamrock, A.M. Herring, ECS Trans. 3 (2006) 551–559.
[76] M. Watanabe, K. Tsurumi, T. Mizukami, T. Nakamura, P. Stonehart, J. Electrochem. Soc. 141 (1994) 2659–2668.
[77] T. Akita, A. Taniguchi, J. Maekawa, Z. Siroma, K. Tanaka, M. Kohyama, K. Yasuda, J. Power Sources 159 (2006) 461–467.
[78] Y. Zhai, H. Zhang, D. Xing, Z. Shao, J. Power Sources 164 (2007) 126–133.
[79] P. Ascarelli, V. Contini, R. Giorgi, J. Appl. Phys. 91 (2002) 4556–4561.
[80] Y. Shao, G. Yin, Y. Gao, J. Power Sources 171 (2007) 558–566.
[81] M.S. Wilson, F.H. Garzon, K.E. Sickafus, S. Gottesfeld, J. Electrochem. Soc. 140 (1993) 2872–2877.
[82] N. Sisofo, 4th Annual Inter. Fuel Cell Testing Workshop, Vancouver, BC, Canada, September 12–13, 2007.
[83] A. Taniguchi, T. Akita, K. Yasuda, Y. Miyazaki, J. Power Sources 130 (2004) 42–49.
[84] L.M. Roen, C.H. Paik, T.D. Jarvi, Electrochem. Solid-State Lett. 7 (2004) A19–A22.
[85] M.F. Mathias, R. Makharia, H.A. Gasteiger, J.J. Conley, T.J. Fuller, G.J. Gittleman, S.S. Kocha, D.P. Miller, C.K. Mittelsteadt, T. Xie, S.G. Yan, P.T. Yu, Electrochem. Soc. Interf. 14 (2005) 24–35.
[86] A.A. Pesaran, G.H. Kim, J.D. Gonder, Milestone report NREL/MP-540-38760, September 2005, at: http://www.nrel.gov/hydrogen/pdfs/pem_fc_freeze_milestone.pdf (accessed December 2007).
[87] R.L. Borup, J.R. Davey, F.H. Garzon, D.L. Wood, M.A. Inbody, J. Power Sources 163 (2006) 76–81.
[88] W.S. Wheat, M.A. Meltser, D.A. Masten, US Patent 6,727,013 (September 7, 2004).
[89] R.J. Assarabowski, W.T. Unkert, L.A. Bach, A.P. Grasso, B.C. Olsommer, US Patent 6,797,421 (January 11, 2004).
[90] K. Wakabayashi, Y. Iwasaki, European Patent 1,414,090 (April 28, 2004).
[91] S. Makino, Japanese Patent 2,004,111,243 (April 8, 2004).
[92] K. Aramaki, Japanese Patent 2,004,047,210 (February 12, 2004).
[93] H.R. Colón-Mercado, B.N. Popov, J. Power Sources 155 (2006) 253–263.
[94] H.A. Gasteiger, S.S. Kocha, B. Sompalli, F.T. Wagner, Appl. Catal. B 56 (2005) 9–35.
[95] T. Toda, H. Igarashi, H. Uchida, M. Watanabe, J. Electrochem. Soc. 146 (1999) 3750–3756.
[96] T. Toda, H. Igarashi, M. Watanabe, J. Electroanal. Chem. 460 (1999) 258–262.
[97] L.J. Wan, T. Moriyama, M. Ito, H. Uchida, M. Watanabe, Chem. Commun. 1 (2002) 58–59.
[98] P. Yu, M. Pemberton, P. Plasse, J. Power Sources 144 (2005) 11–20.
[99] J. Zhang, K. Sasaki, E. Sutter, R.R. Adzic, Science 315 (2007) 200–222.
[100] S.C. Roy, A.W. Harding, A.E. Russell, K.M. Thomas, J. Electrochem. Soc. 144 (1997) 2323–2328.
[101] X.G. Li, S.H. Ge, C.L. Hui, I.M. Hsing, Electrochem. Solid-State Lett. 7 (2004) A286–A289.
[102] Y.Y. Shao, G.P. Yin, Y.Z. Gao, P.F. Shi, J. Electrochem. Soc. 153 (2006) A1093–A1097.
[103] C.Z. He, S. Desai, G. Brown, S. Bollepalli, Electrochem. Soc. Interf. 14 (2005) 41–44.
[104] S. Ye, M. Hall, H. Cao, P. He, ECS Trans. 3 (2006) 657–666.
[105] R. Borup, J. Davey, D. Wood, F. Garzon, M. Inbody, D. Guidry, PEM fuel cell durability, DOE Hydrogen Program, FY 2004 Progress Report.
[106] J. Frisk, W. Boand, M. Hicks, M. Kurkowski, R. Atanasoski, A. Schmoeckel, 2004 Fuel Cell Seminar San Antonio, TX, USA, November 1–5, 2004.
[107] K.H. Kangasniemi, D.A. Condit, T.D. Jarvi, J. Electrochem. Soc. 151 (2004) E125–E132.
[108] C. Lee, W. Mérida, J. Power Sources 164 (2007) 141–153.
[109] M. Schulze, N. Wagner, T. Kaz, K.A. Friedrich, Electrochim. Acta 52 (2007) 2328–2336.
[110] R.L. Borup, Fuel Cell Durability Conference, Washington, DC, USA, December 8–9, 2005.
[111] V. Mehta, J.S. Cooper, J. Power Sources 114 (2003) 32–53.
[112] K. Roßerg, V. Trapp, in: W. Vielstich, H.A. Gasteiger, A. Lamm (Eds.), Handbook of Fuel Cells: Fundamentals Technology and Applications, vol. 3, John Wiley & Sons Ltd., 2003, pp. 308–314.
[113] http://www.hydrogen.energy.gov/annual_review06_fuelcells.html#bipolar (accessed December 2007).
[114] F. de Bruijn, Green Chem. 7 (2005) 132–150.
[115] J. Wind, A. LaCroix, S. Braeuninger, P. Hedrich, C. Heller, M. Schudy, in: W. Vielstich, H.A. Gasteiger, A. Lamm (Eds.), Handbook of Fuel Cells: Fundamentals, Technology and Applications, vol. 3, John Wiley & Sons Ltd., 2003, pp. 294–307.
[116] G.O. Mepsted, J.M. Moore, in: W. Vielstich, H.A. Gasteiger, A. Lamm (Eds.), Handbook of Fuel Cells: Fundamentals, Technology and Applications, vol. 3, John Wiley & Sons Ltd., 2003, pp. 286–293.
[117] D.J.L. Brett, N.P. Brandon, J. Fuel Cell Sci. Technol. 4 (2007) 29–44.
[118] X.Z. Yuan, H.J. Wang, J.J. Zhang, D.P. Wilkinson, J. New Mater. Electrochem. Syst. 8 (2005) 257–269.
[119] F. Barbir, PEM Fuel Cell: Theory and Practice, Elsevier Academic Press, New York, 2005, pp. 99–113.
[120] J. Wind, R. Späh, W. Kaiser, G. Böhm, J. Power Sources 105 (2002) 256–260.
[121] L. Ma, S. Warthesen, D.A. Shores, J. New Mater. Electrochem. Syst. 3 (2000) 221–228.
[122] H. Tawfik, Y. Hung, D. Mahajan, J. Power Sources 163 (2007) 755–767.
[123] M.C. Kimble, A.S. Woodman, E.B. Anderson, American Electroplaters and Surface Finishers Society 1999, AESF SUR/FIN'99 Proceedings, June 21–24, 1999.
[124] P.L. Hentall, J.B. Lakeman, G.O. Mepsted, P.L. Adcock, J.M. Moore, J. Power Sources 80 (1999) 235–241.
[125] L. Gladczuk, C. Joshi, A. Patel, J. Guiheen, Z. Iqbal, M. Sosnowski, Mater. Res. Symp. Proc. 756 (2003) 423–428.
[126] Y. Li, W.J. Meng, S. Swathirajan, S.J. Harris, G.L. Doll, US Patent 5,624,769 (December 22, 1995).
[127] T. Matsumoto, J. Niikura, H. Ohara, M. Uchida, H. Gyoten, K. Hatoh, E. Yasumoto, T. Kanbara, K. Nishida, Y. Sugawara, European Patent 1,094,535 (April 25, 2001).
[128] M.P. Brady, B. Yang, H. Wang, J.A. Turner, K.L. More, M. Wilson, F. Garzon, J. Met. Miner. Mater. Soc. 58 (2006) 50–57.
[129] M.P. Brady, K. Weisbrod, C. Zawodzinski, I. Paulauskas, R.A. Buzhanan, L.R. Walker, Electrochem. Solid-State Lett. 5 (2002) A245–A247.
[130] M.P. Brady, K. Weisbrod, I. Paulauskas, R.A. Buzhanan, K.L. More, H. Wang, M. Wilson, F. Garzon, L.R. Walker, Scripta Mater. 50 (2004) 1017–1022.
[131] I.E. Paulauskas, M.P. Brady, H.M. Meyer III, R.A. Buchanan, L.R. Walker, Corros. Sci. 48 (2006) 3157–3171.
[132] H. Wang, M.P. Brady, G. Teeter, J.A. Turner, J. Power Sources 138 (2004) 86–93.
[133] H. Wang, J.A. Turner, J. Power Sources 128 (2004) 193–200.
[134] M.P. Brady, H. Wang, B. Yang, J.A. Turner, M. Bordignon, R. Molins, M. Abd Elhamid, L. Lipp, L.R. Walker, Int. J. Hydrogen Energy 32 (2007) 3778–3788.
[135] H. Wang, M.A. Sweikart, J.A. Turner, J. Power Sources 115 (2003) 243–251.
[136] R.F. Silva, D. Franchi, A. Leone, L. Pilloni, A. Masci, A. Pozio, Electrochim. Acta 51 (2006) 3592–3598.
[137] Y. Wang, D.O. Northwood, Int. J. Hydrogen Energy 32 (2007) 895–902.
[138] M. Li, S. Luo, C. Zeng, J. Shen, H. Lin, C. Cao, Corros. Sci. 46 (2004) 1369–1380.
[139] K. Natesan, R.N. Johnson, Surf. Coat. Technol. 33 (1987) 341–351.
[140] I. Zafar, R. Timothy, J.V. Guiheeen, N. Dave, World Patent 0,128,019 (April 19, 2001).
[141] R. Borup, N. Vanderborgh, Mater. Res. Soc. Symp. Proc. 393 (1995) 151–155.
[142] S. Joseph, J.C. McClure, R. Chianelli, P. Pich, P.J. Sebastian, Int. J. Hydrogen Energy 30 (2005) 1339–1344.
[143] A. Taniguchi, K. Yasuda, J. Power Sources 141 (2005) 8–12.
[144] N. Cunningham, D. Guay, J.P. Dodelet, Y. Meng, A.R. Hlil, A.S. Hay, J. Electrochem. Soc. 149 (2002) A905–A911.
[145] M.H. Fronk, R.L. Borup, J.S. Hulett, B.K. Brady, K.M. Cunningham, US Patent 6,372,376 (December 7, 1999).
[146] S.J. Lee, C.H. Huang, Y.P. Chen, J. Mater. Process. Technol. 140 (2003) 688–693.
[147] D. Li, T. Buscher, B.I. Swanson, Chem. Mater. 6 (1994) 803–810.
[148] A. Woodman, E. Anderson, K. Jayne, M. Kimble, Development of corrosion-resistant coatings for fuel cell bipolar plates, at: http://www.psicorp.com/publications/PDF/sr-0979.pdf (accessed December 2007).
[149] G. Hinds, Performance and Durability of PEM Fuel Cells: A Review, NAT. PHYS. LAB, Teddington, UK, 2004.
[150] D.R. Hodgson, E. Farndon, US Patent Application 20,030,170,526 (February 4, 2003).
[151] S.J. Lee, C.H. Huang, J.J. Lai, Y.P. Chen, J. Power Sources 131 (2004) 162–168.
[152] R.J. Lawrence, US Patent 4,214,969 (July 29, 1980).
[153] E.N. Balko, R.J. Lawrence, US Patent 4,339,322 (July 13, 1982).
[154] E. Middelman, US Application Patent 20,030,160,352 (April 4, 2003).
[155] C. Del-Río, M.C. Ojeda, J.L. Acosta, M.J. Escudero, E. Hontañón, L. Daza, J. Appl. Polym. Sci. 83 (2004) 2817–2822.

[156] H. Wolf, M. Willert-porada, J. Power Sources 153 (2006) 41–46.
[157] M. Wu, L.L. Shaw, J. Power Sources 136 (2004) 37–44.
[158] A. Pellegri, P.M. Spaziante, US Patent 4,197,178 (April 8, 1980).
[159] R.C. Emanuelson, W. Luoma, W. Taylor, US Patent 4,301,222 (November 17, 1981).
[160] W.A. Taylor, US Patent 4,592,968 (June 3, 1986).
[161] Jr. Stewart, C. Robert, US Patent 4,679,300 (June 2, 1987).
[162] T. Uemura, S. Murakami, US Patent 4,737,421 (April 12, 1988).
[163] M.S. Wilson, D.N. Busick, US Patent 6,248,467 (June 19, 2001).
[164] H.C. Kuan, C.C.M. Ma, K.H. Chen, S.M. Chen, J. Power Sources 134 (2004) 7–17.
[165] T.M. Besmann, J.W. Klett, J.J. Henry Jr., E. Lara-Curzio, J. Electrochem. Soc. 147 (2000) 4083–4086.
[166] T.M. Besmann, J.J. Henry Jr., E. Lara-Curzio, J.W. Klett, D. Hack, K. Butcher, Mater. Res. Soc. Symp. Proc. 756 (2003) FF7.1.1–FF7.1.8.
[167] E.A. Cho, U.S. Jeon, H.Y. Ha, S.A. Hong, I.H. Oh, J. Power Sources 125 (2004) 178–182.
[168] H.J. Li, X.H. Hou, Y.X. Chen, Carbon 38 (2000) 423–427.
[169] S.K. Ryu, T.S. Hwang, S.G. Lee, S.A. Lee, C.S. Kim, Carbon Sci. 2 (2001) 165–169.
[170] J.S. Cooper, J. Power Sources 129 (2004) 152–169.
[171] M. Schulze, T. Knöri, A. Schneider, E. Gülzow, J. Power Sources 127 (2004) 222–229.
[172] J. Tan, Y.J. Chao, J.W. Van Zee, W.K. Lee, Mater. Sci. Eng. A 445/446 (2007) 669–675.
[173] Z. Xie, N. Titichai, K. Shi, S. Holdcroft, Fuel Cell Durability Conference, Washington, DC, USA, December 8–9, 2005.
[174] B. Du, Q. Guo, R. Pollard, D. Rodriguez, C. Smith, J. Elter, J. Met. Miner. Mater. Soc. 58 (2006) 45–49.
[175] J.F. Wu, X.Z. Yuan, J.J. Martin, H.J. Wang, X.T. Bi, P.C. Pei, H.Y. Huang, Proceedings of Hydrogen & Fuel Cell 2007, Vancouver, BC, Canada, May, 2007, pp. 448–458.
[176] T.G. Benjamin, High Temperature Membrane Working Group Meeting, Washington, DC, USA, May 14, 2007.
[177] DOE cell component accelerated stress test protocols for PEM fuel cells, at: http://www1.eere.energy.gov/hydrogenandfuelcells/fuelcells/components.html (accessed December 2007).
[178] S. Knights, 4th Annual International Fuel Cell Testing Workshop, Vancouver, BC, Canada, September 12–13, 2007.
[179] K.L. More, 2005 DOE H_2 Program Review Proceedings, May 2005.
[180] V.A.T. Dam, F.A. de Bruijn, J. Electrochem. Soc. 154 (2007) B494–B499.
[181] T. Rockward, 2007 DOE H_2 Program Review Proceedings, May 2007.
[182] R. Hornung, G. Kappelt, J. Power Sources 72 (1998) 20–21.
[183] J.S. Kim, W.H.A. Peelen, K. Hemmes, R.C. Makkus, Corros. Sci. 44 (2002) 635–655.
[184] S.J. Lee, J.J. Lai, C.H. Huang, J. Power Sources 145 (2005) 362–368.
[185] S.J. Lee, Y.P. Chen, C.H. Huang, J. Power Sources 145 (2005) 369–375.